

## Effects of the indirect transitions on optical dispersion relations

Sadao Adachi

*Department of Electronic Engineering, Faculty of Engineering, Gunma University, Kiryu-shi, Gunma 376, Japan*

(Received 5 July 1989)

We report generalized expressions for the indirect-band-gap contribution to the real ( $\epsilon_1$ ) and imaginary parts ( $\epsilon_2$ ) of the dielectric function of semiconductors. The  $\epsilon_2$  spectrum is assumed to yield a continuous absorption obeying the well-known power law of  $(\hbar\omega - E_g^{\text{id}})^2$  and have a steep high-energy end at the high-energy cutoff  $E_c$ . The corresponding  $\epsilon_1$  spectrum shows no clear structure at the  $E_g^{\text{id}}$  edge, but a strong negative peak at the  $E_c$ . Analyses are presented on the optical dispersion relations of InP at 30 K, and results are in satisfactory agreement with the experimental data over the entire range of photon energies (0–6.0 eV). With use of this model it is possible to analyze the optical dispersion relations in a large number of semiconductors, such as Si, GaP, AlSb, and CdSe.

### I. INTRODUCTION

In a series of earlier papers<sup>1–7</sup> we have demonstrated a method for calculation of the dielectric function,  $\epsilon(\omega) = \epsilon_1(\omega) + i\epsilon_2(\omega)$ , of the diamond-type (Si, Ge, and  $\alpha$ -Sn) and zinc-blende-type semiconductors (GaP, InAs,  $\text{Al}_x\text{Ga}_{1-x}\text{As}$ ,  $\text{In}_{1-x}\text{Ga}_x\text{As}_y\text{P}_{1-y}$ , etc.). An excellent agreement has been achieved between our model and experimental data over the entire range of photon energies ( $E = 0$ –6.0 eV).

We have also studied the excitonic effects on the optical spectra in semiconductors of GaAs (Ref. 8) and InP.<sup>9</sup> Excitonic states should exist at each type of critical points (CP's), since the Coulomb interaction is always present between the electrons and the holes. The effects may profoundly modify the CP singularity structure especially at low temperatures. It has been found<sup>8,9</sup> that the inclusion of the excitonic effects in the one-electron band model corrects the strength of the  $\epsilon(\omega)$  peaks in the correct direction with the experimental information.

It is well known that not only the direct transitions at the CP's but also the indirect transitions at the indirect band gap influence the optical dispersion relations of semiconductors. The indirect transitions in indirect-band-gap materials (e.g., GaP) take part at energies below the onset of the direct transitions, and vice versa at above the onset of the direct transitions in direct-band-gap materials (e.g., InP). Because the indirect transitions are higher order in the perturbation than the direct ones, their strength is usually very weak, and it can only expect to realize them in a spectrum below the direct threshold as a tail of the direct absorption edge in the indirect-band-gap materials. Our previous works,<sup>1–7</sup> however, required a considerable strength of the indirect-band-gap contribution for the analyses of the  $\epsilon_2(\omega)$  spectrum both in the indirect- and direct-band-gap materials. Unfortunately, at that stage we did not have any expression for the contribution to  $\epsilon_1(\omega)$  of the indirect transitions, and thus we took into account its contribution only to  $\epsilon_2(\omega)$ , but not to  $\epsilon_1(\omega)$ .

In this paper we obtain an analytical expression of the indirect-band-gap contribution to  $\epsilon_1(\omega)$  in semiconductors. Although its contribution to  $\epsilon_2(\omega)$  (or absorption coefficient) is well authorized, an expression for  $\epsilon_1(\omega)$  has not yet been reported to our knowledge. We analyze the optical dispersion relations of  $\epsilon(\omega)$  for InP (at 30 K) and obtain an excellent agreement between our model and the experimental data over a wide range of the photon energy.

### II. MODEL

A wide variety of theoretical calculations and experiments have given detailed information about the electronic energy-band structures of semiconductors. We reproduce in Fig. 1 the energy-band structure of InP calculated by an empirical nonlocal pseudopotential method [Chelikowsky and Cohen (Ref. 10)]. The lowest direct absorption edges of InP are 1.415 eV ( $E_0$ ) and 1.521 eV

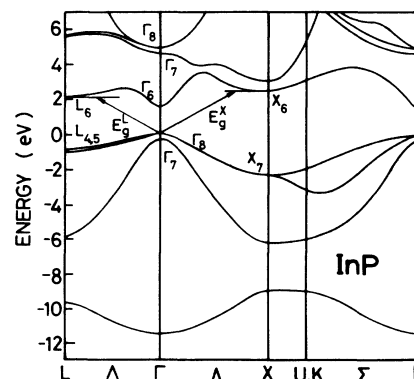


FIG. 1. Electronic energy-band structure of InP along several lines of high-symmetry directions [Chelikowsky and Cohen (Ref. 10)].

( $E_0 + \Delta_0$ ) at 30 K. The lowest indirect absorption edges  $E_g^L$  ( $\Gamma_8^v \rightarrow L_6^c$ ) and  $E_g^X$  ( $\Gamma_8^v \rightarrow X_6^c$ ) are, respectively, 2.05 and 2.21 eV (see Fig. 1). The indirect transitions in InP thus take part above the onset of the lowest direct transitions.

The optical transition mechanism at the indirect band gap,  $E_g^{\text{id}}$ , is expressed by a second-order process in the perturbation.<sup>11</sup> This perturbation gives the contribution of the indirect transitions to  $\epsilon_2(\omega)$  as

$$\epsilon_2(\omega) = \frac{D}{(\hbar\omega)^2} (\hbar\omega - E_g^{\text{id}} + \hbar\omega)^2 \Theta(1 - x_g), \quad (1)$$

with

$$D = \sum_{\beta} \left| \sum_{\alpha} \frac{\langle \beta | H_{eL} | \alpha \rangle \langle \alpha | H_{eR} | 0 \rangle}{E_{\alpha}(k_1) - E_v(k_1) - \hbar\omega} \right|^2, \quad (2)$$

$$x_g = (E_g^{\text{id}} - \hbar\omega_q) / \hbar\omega, \quad (3)$$

$$\Theta(z) \equiv \begin{cases} 1 & \text{for } z \geq 0 \\ 0 & \text{for } z < 0. \end{cases} \quad (4)$$

In Eq. (2)  $H_{eR}$  is the electron-radiation perturbation,  $H_{eL}$  is the electron-lattice perturbation,  $|0\rangle$  is the electronic ground state,  $|\alpha\rangle$  is the intermediate state in the conduction band ( $k = k_1$  and energy  $E_{\alpha}$ ), and the  $|\beta\rangle$  is the final state in the conduction band ( $k = k_2$ ). The mechanism considered is that the valence electron is scattered to the conduction state and a photon of energy  $\hbar\omega$  and a phonon of momentum  $q = k_2 - k_1$  (and energy  $\hbar\omega_q$ ) are both absorbed. The phonon-emission process remains possible, however, the only difference from the above case is the sign of the phonon energy.

The parabolic bands extending to infinite energies implied by Eq. (1) should be nonphysical. We thus modify the model by taking into account a cutoff at the energy  $E_c$ . This modification provides

$$\epsilon_2(\omega) = \frac{D}{(\hbar\omega)^2} (\hbar\omega - E_g^{\text{id}} + \hbar\omega_q)^2 \Theta(1 - x_g) \Theta(1 - x_c), \quad (5)$$

with

$$x_c = \hbar\omega / E_c. \quad (6)$$

Assuming that the strength term  $D$  is independent of the photon energy, the Kramers-Kronig transformation of Eq. (5) gives

$$\begin{aligned} \epsilon_1(\omega) = \frac{2D}{\pi} & \left[ -\frac{(E_g^{\text{id}})^2}{(\hbar\omega)^2} \ln \left[ \frac{E_c}{E_g^{\text{id}}} \right] \right. \\ & + \frac{1}{2} \left[ 1 + \frac{E_g^{\text{id}}}{\hbar\omega} \right]^2 \ln \left[ \frac{\hbar\omega + E_c}{\hbar\omega + E_g^{\text{id}}} \right] \\ & \left. + \frac{1}{2} \left[ 1 - \frac{E_g^{\text{id}}}{\hbar\omega} \right]^2 \ln \left[ \frac{\hbar\omega - E_c}{\hbar\omega - E_g^{\text{id}}} \right] \right]. \quad (7) \end{aligned}$$

The  $\epsilon_1(\omega)$  spectrum of Eq. (7) exhibits a divergence at  $E_c$  (see Fig. 2). We thus introduce in this expression a lifetime broadening effect in a phenomenological manner by replacing  $\hbar\omega$  by  $\hbar\omega + i\Gamma$ . The contribution of the indirect transitions to  $\epsilon(\omega)$  is finally written as

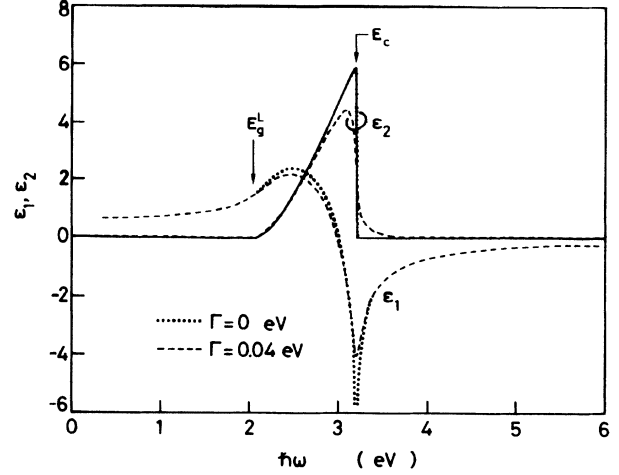


FIG. 2. Line shape of the indirect-band-gap contribution to  $\epsilon(\omega)$  for InP [Eq. (8)] with two different broadening parameters [ $\Gamma = 0$  eV (dotted lines) and 0.04 eV (dashed lines)]. The solid line represents the dependence of  $\epsilon_2$  on  $\omega$  with high-energy cutoff correction in Eq. (5).

$$\begin{aligned} \epsilon(\omega) = \frac{2D}{\pi} & \left[ -\frac{(E_g^{\text{id}})^2}{(\hbar\omega + i\Gamma)^2} \ln \left[ \frac{E_c}{E_g^{\text{id}}} \right] \right. \\ & + \frac{1}{2} \left[ 1 + \frac{E_g^{\text{id}}}{\hbar\omega + i\Gamma} \right]^2 \ln \left[ \frac{\hbar\omega + i\Gamma + E_c}{\hbar\omega + i\Gamma + E_g^{\text{id}}} \right] \\ & \left. + \frac{1}{2} \left[ 1 - \frac{E_g^{\text{id}}}{\hbar\omega + i\Gamma} \right]^2 \ln \left[ \frac{\hbar\omega + i\Gamma - E_c}{\hbar\omega + i\Gamma - E_g^{\text{id}}} \right] \right] \quad (8) \end{aligned}$$

We show in Fig. 2 our calculated  $\epsilon(\omega)$  spectra of Eqs. (5) [ $\epsilon_2(\omega)$ : solid line] and (8) [ $\epsilon_1(\omega) = \text{Re}\epsilon(\omega)$ ;  $\epsilon_2(\omega) = \text{Im}\epsilon(\omega)$ , dotted ( $\Gamma = 0$  eV) and dashed lines ( $\Gamma = 0.04$  eV)]. The numerical values used in the calculations are as follows:  $E_g^{\text{id}} = 2.05$  eV;  $E_c = 3.20$  eV; and  $D = 46.3$ . It is evident from the figure that the  $\epsilon_1$  spectrum exhibits no clear structure at the  $E_g^{\text{id}}$  edge, but a strong negative peak at the cutoff energy  $E_c$ . It is also noteworthy that in the limit  $\Gamma \rightarrow 0$  the  $\epsilon_2$  spectrum of Eq. (8) exactly agrees with that of Eq. (5) (solid line).

The  $E_1$  and  $E_1 + \Delta_1$  transitions in InP may take place along the  $\langle 111 \rangle$  directions ( $\Lambda$ ) or at  $L$  points in the Brillouin zone. These transitions are of the three-dimensional (3D)  $M_1$  [or two-dimensional (2D)  $M_0$ ] type. The contribution to  $\epsilon(\omega)$  of this type of one-electron model is given by (Refs. 1–7)

$$\epsilon(\omega) = [-B_1 x_{1d}^{-2} \ln(1 - x_{1d}^2) - B_2 x_{1sd}^{-2} \ln(1 - x_{1sd}^2)], \quad (9)$$

where

$$x_{1d} = (\hbar\omega + i\Gamma) / E_1, \quad (10)$$

$$x_{1sd} = (\hbar\omega + i\Gamma) / (E_1 + \Delta_1). \quad (11)$$

In Eqs. (9)–(11), the  $B$ 's are the strength parameters of the one-electron model at the 3D- $M_1$  (2D- $M_0$ ) CP's and  $\Gamma$  is a lifetime broadening parameter.

Excitonic states should, in principle, exist at each type of CP, since the Coulomb-like interaction is always present between the electrons and the holes. Optical spectra in the  $E_1/(E_1 + \Delta_1)$  structure region of InP become sharp when the temperature is lowered.<sup>12</sup> Such spectral change cannot be explained within the framework of the one-electron approximation with lifetime broadening corrections. This fact clearly suggests an evidence for the contribution of excitonic effects to the  $E_1/(E_1 + \Delta_1)$  transitions. There may be only two analytical equations which enable us to treat the excitonic effects at the  $E_1/(E_1 + \Delta_1)$  spectral region: (i) the effective-mass (EM) approximation<sup>13,14</sup> and (ii) the Koster-Slater (KS) method.<sup>15,16</sup> Not only the EM approximation but also the KS method dramatically modify and sharpen the  $E_1/(E_1 + \Delta_1)$  CP structure. However, a degree of the sharpness is larger for the EM approximation than for the KS method.<sup>8</sup> We can find a better fit with experiment using the EM approximation than the KS method.

In the case of the 3D- $M_1$  CP's (i.e., saddle-point excitons or hyperbolic excitons), the EM equation is much more difficult to solve. However, in the limit  $m_L^{-1} \approx 0$  ( $m_L$ : the longitudinal effective mass) the equation gives a series of the 2D Wannier-type exciton (discrete exciton)<sup>14</sup>

$$E_{x_1}^n (E_{x_\Delta}^n) = -R_y^{2D} / (n - \frac{1}{2})^2, \quad (12)$$

where  $E_{x_1}^n (E_{x_\Delta}^n)$  is the exciton energy, and  $R_y^{2D}$  is the exciton Rydberg energy. The contribution of the 2D-exciton transitions to  $\epsilon(\omega)$  can now be written with Lorentzian line shape as

$$\epsilon(\omega) = \sum_{n=1}^{\infty} [B_{1x}^n (E_1 + E_{x_1}^n - \hbar\omega - i\Gamma)^{-1} + B_{2x}^n (E_1 + \Delta_1 + E_{x_\Delta}^n - \hbar\omega - i\Gamma)^{-1}], \quad (13)$$

where  $B_{1x}^n$  and  $B_{2x}^n$  are the exciton strength parameters at the  $E_1$  and  $E_1 + \Delta_1$  CP's, respectively. The 2D EM approximation also gives the continuum part of the excitonic states.<sup>14</sup> However, one can consider that the contribution of this part is similar to that of the one-electron approximation [i.e., Eq. (9)]. We thus neglect the continuum-exciton contribution to  $\epsilon(\omega)$  in the present analysis.

The more pronounced structure found in InP in the region higher in energy than  $E_1$  is labeled  $E'_0 (E'_0 + \Delta'_0)$ . The nature of the  $E'_0$  transitions is more complicated, since it does not correspond to a single, well-defined CP. Because of this fact, we shall characterize the  $E'_0$  structure as that of a damped harmonic oscillator (DHO) (Refs. 1–7):

$$\epsilon(\omega) = \frac{C}{(1 - x_2^2) - ix_2\gamma}, \quad (14)$$

with

$$x_2 = \hbar\omega / E'_0, \quad (15)$$

where  $C$  is the strength parameter, and  $\gamma$  is the broadening energy divided by  $E'_0$  (i.e.,  $\gamma = \Gamma / E'_0$ , where  $\Gamma$  is in eV).

Many-particle effects on CP's in the interband continuum of semiconductors have been treated with their detailed electronic-energy band structures.<sup>17,18</sup> Results have shown that the absorption at the  $E'_0 (E_2)$  CP is markedly weakened with no drastic change in its shape by introducing the excitonic interaction. Unfortunately, however, it seems that no analytical line shape suitable to fit the excitonic-effect-influenced  $E'_0$  line shape is reported up to date. We found that for GaAs and InP the DHO model is a good representation for the  $E'_0 (E_2)$  CP both with and without the presence of the excitonic interaction.<sup>8,9</sup>

The  $E_0$  and  $E_0 + \Delta_0$  transitions in the diamond- and zinc-blende-type semiconductors occur in the center of the BZ. These transitions are of the 3D- $M_0$  CP's. Assuming the bands are parabolic, and using the Kramers-Kronig relations, we obtain the contribution of these band gaps to  $\epsilon_2(\omega)$  and  $\epsilon_1(\omega)$  (Refs. 1–7):

$$\begin{aligned} \epsilon_2(\omega) = & [A / (\hbar\omega)^2] [(\hbar\omega - E_0)^{0.5} \Theta(x_0 - 1) \\ & + \frac{1}{2}(\hbar\omega - E_0 - \Delta_0)^{0.5} \\ & \times \Theta(x_{s.o.} - 1)], \end{aligned} \quad (16)$$

$$\epsilon_1(\omega) = AE_0^{-1.5} \{f(x_0) + \frac{1}{2}[E_0 / (E_0 + \Delta_0)]^{1.5} f(x_{s.o.})\}, \quad (17)$$

with

$$A = \frac{4}{3} (\frac{3}{2} m^*)^{1.5} P^2, \quad (18)$$

$$f(x_0) = x_0^{-2} [2 - (1 + x_0)^{0.5} - (1 - x_0)^{0.5} \Theta(1 - x_0)], \quad (19)$$

$$\begin{aligned} f(x_{s.o.}) = & x_{s.o.}^{-2} [2 - (1 + x_{s.o.})^{0.5} \\ & - (1 - x_{s.o.})^{0.5} \Theta(1 - x_{s.o.})], \end{aligned} \quad (20)$$

$$x_0 = \hbar\omega / E_0, \quad (21)$$

$$x_{s.o.} = \hbar\omega / (E_0 + \Delta_0), \quad (22)$$

where  $m^*$  is the combined density-of-states mass,  $P^2$  is the squared momentum matrix element, and  $H$  is a function defined by Eq. (4).

It is well known<sup>19</sup> that the discrete lines and continuum excitons in the neighborhood of the lowest direct band edge (3D- $M_0$  CP) dramatically change the optical spectrum. However, the discrete-exciton states are present only in the limited region close to the  $E_0$  edge and their strength is considerably weaker than those of the ensuing  $E_1$ ,  $E_1 + \Delta_1$ , and  $E'_0$ . Also, the continuum-exciton transitions at the 3D- $M_0$  CP behave like the one-electron characteristics [Eqs. (16) and (17)]. The excitonic effects at the  $E_0/(E_0 + \Delta_0)$  edges are thus not so important and can be neglected in the following analysis.

### III. COMPARISON OF OUR MODEL TO EXPERIMENTAL SPECTRA

The model given in Sec. II can be used to fit the experimental dispersion of  $\epsilon_2$  and  $\epsilon_1$  over most of the spectral

range (0–6.0 eV). The parameters, such as  $A$ ,  $B_1$ , and  $C$ , can be commonly used as adjustable constants for the calculation of both  $\epsilon_2$  and  $\epsilon_1$ .

The fit with our model to the experimental  $\epsilon_2$  of InP at 30 K is shown in Fig. 3. The solid line is obtained from the sum of Eqs. (8) ( $\Gamma=0.04$  eV), (9), (13), (14), and (16). The dashed line is the result of the sum of Eqs. (9), (13), (14), and (16) [i.e., without taking account of Eq. (8) (indirect-band-gap contribution)]. The numerical values used in the calculations are as follows:  $E_1=3.28$  eV;  $E_1+\Delta_1=3.42$  eV;  $B_1=3.6$ ;  $B_2=0.9$ ;  $B_{1x}^1=1.0$  eV;  $B_{2x}^1=0.25$  eV;  $R_y^{2D}=0.02$  eV;  $\Gamma=0.08$  eV [Eqs. (9) and (13)];  $E'_0=4.75$  eV;  $C(E'_0)=1.191$ ;  $\gamma(E'_0)=0.070$ ;  $E'_0+\Delta'_0=5.01$  eV;  $C(E'_0+\Delta'_0)=0.306$ ;  $\gamma(E'_0+\Delta'_0)=0.053$ ;  $E_0=1.415$  eV;  $E_0+\Delta_0=1.521$  eV; and  $A=5.4$  eV<sup>1.5</sup>. The indirect-band-gap ( $E_g^L$ ) parameters are the same as those used in Fig. 2. The  $E_g^X$  transitions may also take part at energies above  $E_g^X$  ( $\approx 2.21$  eV). However, the energy difference between  $E_g^L$  and  $E_g^X$  is relatively small ( $\approx 0.16$  eV). This assures that the strength parameter  $D$  ( $E_g^L$ ) can take over the  $E_g^X$  gap strength. Because of this, we considered only the  $E_g^L$  gap contribution as the indirect-band-gap ones. The solid circles are the experimental data taken from Ref. 12.

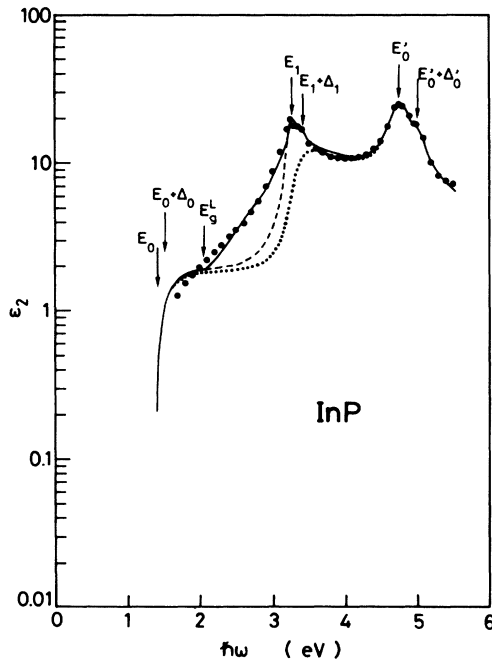


FIG. 3.  $\epsilon_2$  spectrum of InP at 30 K. The solid line is obtained from the sum of Eqs. (8), (9), (13), (14), and (16). The dashed line is the result of the sum of Eqs. (9), (13), (14), and (16) [i.e., without taking account of Eq. (8) (indirect-band-gap contribution)]. The dotted line is also obtained from the sum of Eqs. (9), (14), and (16) [i.e., without taking account of Eqs. (8) and (13) (saddle-point excitons)]. The solid circles are the experimental data taken from Ref. 12.

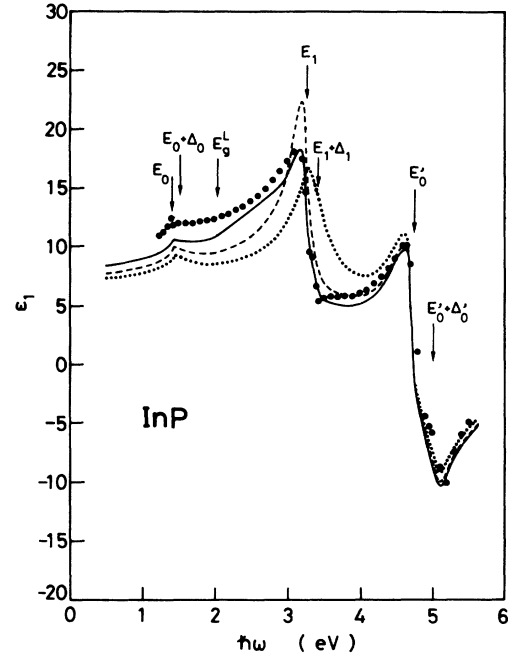


FIG. 4.  $\epsilon_1(\omega)$  spectrum of InP at 30 K. The solid line is obtained from the sum of Eqs. (8), (9), (13), (14), and (17). The dashed line is taken by the sum of Eqs. (9), (13), (14), and (17) [i.e., without taking account of Eq. (8) (indirect-band-gap contribution)]. The dotted line is also taken by the sum of Eqs. (9), (14), and (17) [i.e., without taking account of Eqs. (8) and (13) (saddle-point excitons)]. The solid circles are the experimental data taken from Ref. 12.

There is an accumulation of interband CP's in the energy region of 4.5–5.5 eV. This accumulation consists of the  $E'_0$  and  $E_2$  multiplets. We considered only two DHO's in this region. The dotted line in Fig. 3 is also obtained from the sum of Eqs. (9), (14), and (16) [i.e., without taking account of Eqs. (8) (indirect-band-gap contribution) and (13) (saddle-point excitons)]. It is evident from the figure that the inclusion of this exciton contribution (dashed line) is a great improvement over the one-electron approximation (dotted line). If we do not take into account the indirect-band-gap contribution (dashed line), the fit with the experimental data becomes very poor in the 2–3-eV region. There is a possibility of various indirect-band-gap transitions in InP: they are  $E_g^L$  ( $\Gamma_8^v \rightarrow L_6^c$ ,  $\Gamma_7^v \rightarrow L_6^c$ ),  $E_g^X$  ( $\Gamma_8^v \rightarrow X_6^c$ ,  $\Gamma_7^v \rightarrow X_6^c$ ), etc. (see Fig. 1). The lowest indirect band gap of this material is  $E_g^L \approx 2.05$  eV ( $\Gamma_8^v \rightarrow L_6^c$ ). By taking into account this indirect band gap, we can achieve an excellent agreement between our calculation (solid line) and the experimental data over a wide range of the photon energies.

A comparison of our calculated  $\epsilon_1(\omega)$  to the experimental data of InP at 30 K is shown in Fig. 4. The solid line is obtained from the sum of Eqs. (8) ( $\Gamma=0.04$  eV), (9), (13), (14), and (17). The dashed line is taken by the sum of Eqs. (9), (13), (14), and (17) [i.e., without taking account of Eq. (8)]. The dotted line is also taken by the sum of Eqs. (9), (14), and (17) [i.e., without taking

count of Eqs. (8) and (13)]. The numerical parameters are the same as those used in the case for  $\epsilon_2(\omega)$  (Fig. 3). The solid circles are the experimental data taken from Ref. 12.

As seen in the figure, the dotted line provides a poor fit with the experimental data in the energy region at or below the  $E_1/(E_1+\Delta_1)$  edges. When we put  $\Gamma=0$  eV into Eqs. (9) and (13), the calculated spectrum exhibits a divergence at the  $E_1/(E_1+\Delta_1)$  edges.<sup>1-5</sup> A properly chosen value of  $\Gamma$  can decrease the strength of the  $E_1/(E_1+\Gamma_1)$  peak and leads to a correct direction which is coincident with the experimental verification. However, the calculated  $\epsilon_1$  value with  $\Gamma=0.08$  eV at the  $E_1$  edge is 22.4 (dashed line) while the experimental one is 18.1 (i.e., the calculated  $\epsilon_1$  peak is considerably larger than the experimental one). As in the case for  $\epsilon_2$ , such a disagreement can be successfully removed by taking into account the indirect-band-gap contribution [Eq. (8)] in the calculation for  $\epsilon_1$ . This result is shown in Fig. 4 by the solid line. If we consider the excitonic states at the  $E_0/(E_0+\Delta_0)$  edges, the fit may also be greatly improved especially in the spectral region near these edges.

#### IV. CONCLUSIONS

We have obtained generalized expressions for the indirect-band-gap contribution to the real ( $\epsilon_1$ ) and imaginary parts ( $\epsilon_2$ ) of the dielectric function of semiconductors. The model is based on the Kramers-Kronig transformation and assumes that the  $\epsilon_2$  spectrum yields a continuous absorption obeying the well-known power law of  $(\hbar\omega - E_g^{\text{id}})^2$  and a steep high-energy end at the cutoff energy  $E_c$ . The corresponding  $\epsilon_1$  spectrum shows no clear structure at the  $E_g^{\text{id}}$  edge, but a strong negative peak at the  $E_c$ . Detailed analyses are presented on the optical dispersion relations of InP at 30 K, and results are in satisfactory agreement with the experimental data over the entire range of photon energies (0–6.0 eV). This model can also be applicable to other semiconductors, such as Si, GaP, AlSb (Ref. 20), and CdSe (Ref. 21).

#### ACKNOWLEDGMENTS

It is a pleasure to acknowledge many useful discussions with Dr. H. Aikawa. This work was supported in part by the Gunma University Foundation for Science and Technology, Gunma, Japan.

<sup>1</sup>S. Adachi, Phys. Rev. B **35**, 7454 (1987).

<sup>2</sup>S. Adachi, Phys. Rev. B **38**, 12 345 (1988).

<sup>3</sup>S. Adachi, Phys. Rev. B **38**, 12 966 (1988).

<sup>4</sup>S. Adachi, Phys. Rev. B **39**, 12 612 (1989).

<sup>5</sup>S. Adachi, J. Appl. Phys. **66**, 813 (1989).

<sup>6</sup>S. Adachi, J. Appl. Phys. **66**, 3224 (1989).

<sup>7</sup>S. Adachi, J. Appl. Phys. (to be published).

<sup>8</sup>S. Adachi, Phys. Rev. B **41**, 1003 (1990).

<sup>9</sup>S. Adachi, Jpn. J. Appl. Phys. **28**, 1536 (1989).

<sup>10</sup>J. R. Chelikowsky and M. L. Cohen, Phys. Rev. B **14**, 556 (1976).

<sup>11</sup>S. Adachi and C. Hamaguchi, Physica B+C **97B**, 187 (1979).

<sup>12</sup>P. Lautenschlager, M. Garriga, and M. Cardona, Phys. Rev. B

**36**, 4813 (1987).

<sup>13</sup>E. O. Kane, Phys. Rev. **180**, 852 (1969).

<sup>14</sup>B. Velicky and J. Sak, Phys. Status Solidi **16**, 147 (1966).

<sup>15</sup>J. E. Rowe and D. E. Aspnes, Phys. Rev. Lett. **25**, 162 (1970).

<sup>16</sup>R. M. Martin, J. A. Van Vechten, J. E. Rowe, and D. E. Aspnes, Phys. Rev. B **6**, 2500 (1972).

<sup>17</sup>W. Hank and L. J. Sham, Phys. Rev. B **21**, 4656 (1980).

<sup>18</sup>M. del Castillo-Mussot and L. J. Sham, Phys. Rev. B **31**, 2092 (1985).

<sup>19</sup>R. J. Elliott, Phys. Rev. **108**, 1384 (1957).

<sup>20</sup>S. Adachi (unpublished).

<sup>21</sup>S. Adachi (unpublished).